PROCEEDINGS OF SCIENCE

A SRF Cavity for Gravitational Wave Detection

Lars Fischer,[a,*] **Robin Löwenberg,**[a] **Gudrid Moortgat-Pick,**[a,b] **Michel Paulsen,**[a] **Krisztian Peters**[b] **and Marc Wenskat**[c]

[a] *Universität Hamburg, Institute of Theoretical Physics, Luruper Chaussee 149, 22761 Hamburg, Germany*

[b] *Deutsches-Elektronen-Synchrotron (DESY), Notkestraße 85, 22761 Hamburg, Germany*

[c] *Universität Hamburg, Institute for Experimental Physics, Luruper Chaussee 149, 22761 Hamburg, Germany*

E-mail: lars.fischer@desy.de, gudrid.moortgat-pick@desy.de

This study focuses on the detection of gravitational waves (GW) in the high frequency regime with superconducting radio frequency (SRF) cavities. Measurements in the intended frequency range O(kHz-GHz) could give possible hints to new physics beyond the standard model and insights into previously hidden early universe phenomena.
The detection principle is based on the transition between two electromagnetic eigenmodes of a SRF cavity and can be described by a direct and an indirect interaction of gravitational waves with the electromagnetic field. The indirect coupling coefficients with the cavity shell are precisely analyzed and additionally the Gertsenshtein effect governing the direct interaction is presented.
In order to improve the description of GW detection, we apply our results to a SRF cavity prototype built by the MAGO collaboration at INFN Genoa in the early 2000s. Together with FNAL the Universität Hamburg and DESY revisit research on this detector concept by characterizing its geometry and the corresponding mechanical and electromagnetic eigenmodes. Combined with numerical simulations the GW strain sensitivity is calculated in the desired frequency range. Further improvements on the MAGO cavity prototype parameters indicate that the region of new physics is accessible.

The European Physical Society Conference on High Energy Physics (EPS-HEP2023)
21-25 August 2023
Hamburg, Germany

*Speaker

PoS(EPS-HEP2023)077

1. Introduction

After the first observation of gravitational waves (GW) by the LIGO and VIRGO collaborations [1] a new field of observational astrophysics gained access to analyse previously partially hidden phenomena. Especially new strong evidence for a stochastic gravitational wave background in the nano Hertz regime found in pulsar timing array (PTA) data by the NANOGrav collaboration [2] excited new interest in GW search in the high frequency regime [3]. Observations of GW with frequencies beyond 10 kHz would most certainly point to new physics because the standard model does not predict sources for this frequency regime. Recent studies [4, 5] revisiting the heterodyne GW experiments with superconducting radio frequency (SRF) cavities show sensitivities reaching areas of possible new physics. The concept was initially developed theoretically in the late 1970s [6–8] and experimental efforts in the early 2000s by the MAGO collaboration [9, 10] resulted in the construction of two prototype cavities. Now, almost 20 years after the project has been stopped, FNAL, INFN Genoa, DESY and the Universität Hamburg reactivate the project and collaborate on a proof of concept study with one of the prototype cavities built by the MAGO collaboration.

The fundamental detection principle is based on two nearly degenerate electromagnetic eigenmodes of the coupled microwave cavity system. The energetically lower eigenmode is excited by a narrow external oscillator (pump mode) to store RF energy inside the cavity. A sensitive readout system is coupled to the other energetically higher eigenmode and measures the electromagnetic field spectral power around the carrier frequency. The passage of a GW can induce photon transitions from the pump mode to the signal mode. The maximal energy transfer is reached when the GW frequency is on resonance with the frequency difference of the pump and signal modes. Thus heterodyne SRF cavity experiments have the ability to scan over a large GW frequency range reaching from 1 kHz to a few GHz. In the superconducting state the cavity has very high electromagnetic quality factors ($Q \sim 10^{10} - 10^{12}$) which are necessary to resolve the frequency difference in the kHz regime.

The interaction of a GW with the EM field of the pump mode can be described by two independent phenomena. A direct coupling via the Gertsenshtein effect [11, 12] dominant only for high GW frequencies above 1 GHz. It will not be of relevance for the existing prototype, but it is introduced for completeness. The indirect interaction of a GW with the detector displaces the cavity shell and thus induces an overlap of pump and signal mode also causing energy to be transferred to the signal mode. All calculations in this analysis are done in the well known long-wavelength approximation, where the GW wavelength is much longer than than the detectors size.

2. The Gertsenshtein Effect

In the 1960s Mikhail E. Gertsenshtein discovered that an electromagnetic wave with ω_{em} propagating through a static transverse magnetic field can induce a GW with the same frequency [11]. This interaction also works in the opposite direction, a GW with ω_g propagating through an electromagnetic field induces photons of the frequency $\omega = \omega_g + \omega_{em}$. In the framework of linearized theory of gravity, where GW are usually derived, the general metric can be decomposed in a minkowskian and a perturbative part, i.e. $g_{\mu\nu} = \eta_{\mu\nu} + h_{\mu\nu}$. We assume that the perturbation,

also known as the GW strain tensor, is small i.e. $|h_{\mu\nu}| \ll 1$ and $|\partial_\alpha h_{\mu\nu}| \ll 1$. Throughout all derivations we use the convention $(-,+,+,+)$ for $\eta_{\mu\nu}$.

The GW interaction with electromagnetic fields is derived from the Einstein-Maxwell action, with $j_\mu = 0$ in vacuum. The strain $h_{\mu\nu}$ induces an additional effective current in the modified Maxwell equations

$$j^\mu_{\text{eff}} = \partial_\nu(\frac{1}{2}h^\alpha_{\ \alpha}F^{\mu\nu} + h^\nu_{\ \alpha}F^{\alpha\mu} - h^\mu_{\ \alpha}F^{\alpha\nu}), \tag{1}$$

which, however, does not transform covariantly like a four-vector [5, 13]. Thus a fixed frame of reference must be chosen to evaluate the strain, where the most convenient choice turns out to be the proper detector (PD) frame [13]. However, GW have the simplest form in the transverse-traceless (TT) gauge and therefore we assume monochromatic GW of frequency ω_g propagating in z-direction. They can be express in the TT-gauge as

$$h^{TT}_{ij,z}(t) = \begin{pmatrix} h_+ & h_\times & 0 \\ h_\times & -h_+ & 0 \\ 0 & 0 & 0 \end{pmatrix} e^{i\omega_g t}, \tag{2}$$

where $h_\times$ and h_+ denote the polarization states of GW. In the long-wavelength regime the strain in the PD has only one non-zero component which is related to the TT-gauge representation via $h^{PD}_{00} = \frac{1}{2}\ddot{h}^{TT}_{ij}(g)x^i x^j$, with g denoting the geodesic of the detector. From the modified Maxwell equations the induced current density $\vec{j}_{\text{eff}}$ can be derived in the PD frame and has the form

$$\vec{j}_{\text{eff}} = -\frac{1}{2}\partial_t(h_{00}\vec{E}_0) - \frac{1}{2}\nabla \times (h_{00}\vec{B}_0), \tag{3}$$

where $\vec{E}_0$ and $\vec{B}_0$ are the electromagnetic fields of the pump mode in the cavity. From the effective current the direct coupling coefficients η^E_{01} and η^B_{01} can be derived (see Eq.18) in chapter 4.

3. Cavity Wall Deformation

The indirect interaction of a GW deforms the cavity walls and changes the boundary conditions for the electromagnetic field modes. The cavity deformation can be derived from classical elastic theory and has been done in [10, 15]. In general, the deformation due to an external force density $\vec{f}(t,\vec{x})$ is explained by the equations of motion for isotropic elastic solids

$$\vec{f}(t,\vec{x}) = \rho(\vec{x})\frac{\partial^2\vec{u}}{\partial t^2} - \mu\Delta\vec{u} - (\lambda+\mu)\vec{\nabla}(\vec{\nabla}\cdot\vec{u}). \tag{4}$$

The parameters λ and μ are the first and second Lamé coefficients of the material and $\rho(\vec{x})$ the material density. With a standard separation ansatz $\vec{u}(t,\vec{x}) = \sum_l \vec{\xi}_l(\vec{x})q_l(t)$ the equations of motion for the $q_l(t)$ can be derived

$$\ddot{q}_l(t) + \omega_l^2 q_l(t) = f_l(t)/M. \tag{5}$$

In case of passing GW, $\vec{f}(t,\vec{x})$ is a tidal force density derived from the equation of geodesic deviation [16]

$$\vec{f}(t,\vec{x}) = -\rho(\vec{x})R_{0i0j}(t)x^j\vec{e}^i, \tag{6}$$

where R_{0i0j} denotes the Riemann curvature tensor.

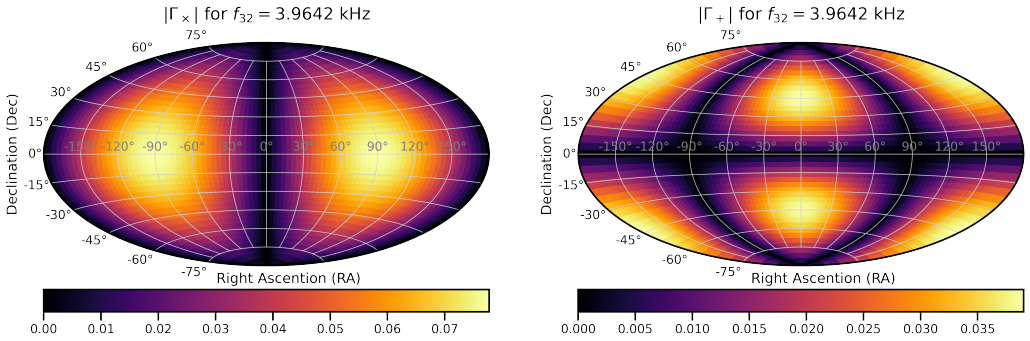

Figure 1: Due to the symmetry of the MAGO detector prototype, mechanical quadrupole modes are excited when GW come from certain directions. This can be seen in the above plots where on the left (right) the normalized coupling coefficient are shown for the pure polarization state $h_\times$ (h_+) of monochromatic GW from arbitrary directions. The GW propagates along the coupling tube of the cavity (see figure 2) if Declination and Right Ascention are zero. Mode $f_{32} = 3.96\,\text{kHz}$ refers to the lowest mechanical quadrupole mode of the ideal MAGO prototype geometry. These simulations were done with COMSOL multiphysics.

3.1 Coupling coefficient GW-mechanical Modes

The MAGO cavity geometry, with the main features shown in figure 2, was developed by the MAGO collaboration [9] and is based on two orthogonal oriented elliptical cells to induce the intended electromagnetic field polarization for GW detection [13]. The central tuning cell was designed to be mechanically deformed and tune the frequency splitting in range $4\,\text{kHz} \leq \omega_1 - \omega_0 \leq 10\,\text{kHz}$. The z axis points along the coupling tube between the two elliptical cells.

For monochromatic GW in z-direction we can plug in Eq.6 the expression of the Riemann tensor in the TT-gauge [18], it is invariant under gauge transformations. With the generalised definition of a force density $f_l(t) := \int_V d^3x \vec{f}(t,\vec{x})\vec{\xi}_l(\vec{x})$ for mechanical mode l with $\vec{\xi}_l(\vec{x})$ a normalized vector field for the deformation of the cavity shell, we derive from Eq.6

$$f_l(t) = -\frac{\omega_g^2}{2} M_{\text{cav}} V_{\text{cav}}^{1/3} (h_+ \Gamma_+^l + h_\times \Gamma_\times^l) e^{i\omega_g t}, \tag{7}$$

where M_{cav} denotes the cavity mass, V_{cav} the cavity volume and we have defined the dimensionless coupling coefficients Γ_+^l and $\Gamma_\times^l$ that express the interaction strength of GW with the l^{th} mechanical mode. They are defined as

$$\Gamma_+^l := V_{\text{cav}}^{-1/3} M_{\text{cav}}^{-1} \int_{V_{\text{cav}}} d^3x \rho(\vec{x}) \left(x\vec{\xi}_{\text{l,x}}(\vec{x}) - y\vec{\xi}_{\text{l,y}}(\vec{x}) \right), \tag{8}$$

$$\Gamma_\times^l := V_{\text{cav}}^{-1/3} M_{\text{cav}}^{-1} \int_{V_{\text{cav}}} d^3x \rho(\vec{x}) \left(x\vec{\xi}_{\text{l,y}}(\vec{x}) + y\vec{\xi}_{\text{l,x}}(\vec{x}) \right). \tag{9}$$

From numerical calculations with COMSOL with the MAGO geometry we found $\Gamma_\times$, Γ_+ to be of order $O(10^{-1})$. In figure 1 the couplings are shown for GW propagating from arbitrary directions of space, i.e. $h_{ij}^{TT}(\alpha,\beta) = \mathcal{R}(\alpha,\beta) h_{ij,z}^{TT} \mathcal{R}^T(\alpha,\beta)$ with $\mathcal{R}(\alpha,\beta) = \mathcal{R}_x(\alpha) \cdot \mathcal{R}_y(\beta)$, a rotation around x- and y-axis.

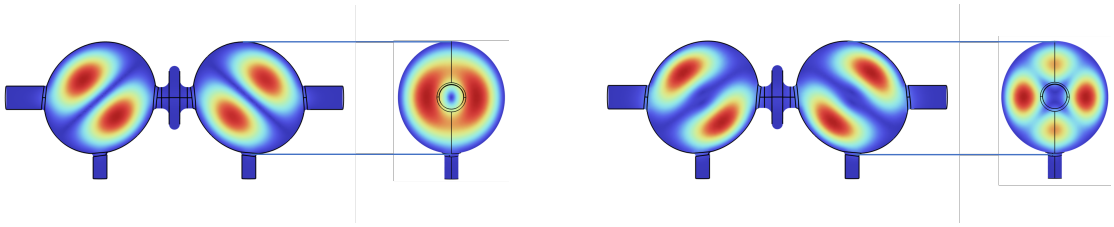

(a) TE_{011} mode at $f_{\text{em}} = 2.103\,\text{GHz}$ **(b)** TE_{111} mode at $f_{\text{em}} = 2.693\,\text{GHz}$

Figure 2: Depending on the pump and signal mode geometry, the coupling to the mechanical vibrations of the cavity shell changes. The MAGO collaboration found a mode at $f_{\text{em}} = 2.1\,\text{GHz}$ to have the strongest coupling and for comparison a mode at $f_{\text{em}} = 2.7\,\text{GHz}$ with similar field distribution has also been tested. For both modes the normalized electric field normal is shown in the yz-plane (left) and xy-plane (right). Red corresponds to electric field maxima and blue to low field values.

3.2 Coupling coefficient Mechanical-EM Mode

The electromagnetic field inside the evacuated cavity follow the wave equations

$$\Delta\vec{E} = \frac{1}{c^2}\frac{\partial^2\vec{E}}{\partial t^2}, \qquad \Delta\vec{B} = \frac{1}{c^2}\frac{\partial^2\vec{B}}{\partial t^2}, \tag{10}$$

where the general solutions can be decomposed in a time and spatial dependent part

$$\vec{E}(t,\vec{x}) = \sum_n e_n(t)\vec{E}(\vec{x}), \qquad \vec{B}(t,\vec{x}) = \sum_n b_n(t)\vec{B}(\vec{x}). \tag{11}$$

In order to express the changing boundary conditions due to the vibrating cavity shell, cavity perturbation theory [17] is applied to first order with $e'_n(t) = e_n(t) + \sigma e_n^{(1)}(t) + O(\sigma^2)$ and $b'_n(t) = b_n(t) + \sigma b_n^{(1)}(t) + O(\sigma^2)$, where $e_n(t)$ and $b_n(t)$ are the time dependent decomposition, Eq.11. The derivation shown in [5] yields the coupling coefficients between the mechanical vibrations of the cavity boundaries and the electromagnetic field

$$C_{01}^l = \frac{V_{\text{cav}}^{1/3}}{2\sqrt{U_0 U_1}} \int_{\partial V_{\text{cav}}} d\vec{S}\cdot\vec{\xi}_l(\vec{x})\left[\frac{1}{\mu_0}\vec{B}_0(\vec{x})\vec{B}_1(\vec{x}) - \epsilon_0\vec{E}_0(\vec{x})\vec{E}_1(\vec{x})\right], \tag{12}$$

where $\vec{B}_0(\vec{x})$, $\vec{E}_0(\vec{x})$ and $\vec{B}_1(\vec{x})$, $\vec{E}_1(\vec{x})$ correspond to the pump and signal mode respectively with U_0 and U_1 the energy stored in each mode.

For the convention of the TE_{lmn} cavity eigenmodes we follow [19], with $2l$ periods in ϕ direction, m half periods along z and n half periods in r direction for cylindrical coordinates with the z axis aligned with the long semi-axis of the elliptical cavities. The MAGO collaboration [9] found that the coupling to the TE_{011} mode maximizes the coefficient in Eq.12. For comparison a TE_{111} mode with similar field distribution has also been investigated (inspired by ref. [13]) and both electromagnetic mode fields are shown in figure 2. To evaluate which mode is suited best for the indirect detection, we multiply the maximum value of the GW mechanical coupling coefficients, Eq.8, with the numerical value for the mechanical EM overlap factor, Eq.12. The values for mechanical eigenmodes between 0.5 kHz and 12 kHz, where the lowest mechanical quadrupole mode is expected, are displayed in figure 3 for the TE_{011} and the TE_{111} mode. The strongest coupling

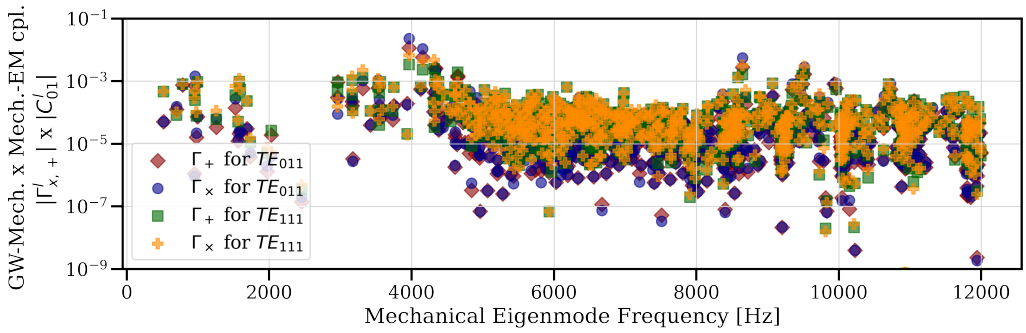

Figure 3: The indirect GW coupling to the output signal is characterized by the product of the coefficients $\Gamma^l_{\times,+}$ and C^l_{01}. First the passing GW displaces the cavity shell and excites mechanical eigenmodes of the cavity which is described by $\Gamma^l_{\times,+}$. The mechanical vibrations then induce a mode overlap of the pump and signal mode, the energy transfer efficiency is described by C^l_{01}. For most of the analysed GW frequency spectrum this product must be maximised to get the highest GW sensitivity.

occurs for a mechanical mode with $f_{\text{mech}} = 3.96\,\text{kHz}$ for both the TE_{011} and TE_{111} mode. However, the coupling at this frequency is dominated by the TE_{011} mode. The TE_{011} modes symmetric and anti-symmetric states are nearly degenerate and will be thus used as pump and signal mode for the detector system.

4. The Equations of Motion

A detailed derivation of the equations of motion including the Gertsenshtein effect can be found in [5], we will only give a brief outline here. In order to take into account the direct and indirect interactions of GW with the heterodyne SRF cavity, electromagnetic and mechanical parts are included in the Lagrangian of the full system,

$$\mathcal{L} = \int_{V_{\text{cav}}} dV \Big(-\frac{1}{4} F_{\mu\nu} F^{\mu\nu} - \frac{1}{2} j^{\mu}_{\text{eff}} A_{\mu} \Big) + \sum \Big(\frac{1}{2} M \dot{q}_l^2(t) - \frac{1}{2} M \omega_l^2 q_l^2(t) + q_l(t) f_l(t) \Big). \tag{13}$$

The equations of motion can be derived for the electromagnetic and mechanical (where we assume only one contributing mechanical mode) dynamics. If we include damping terms and an external oscillator connected to the pump mode with power leakage ϵ to the signal mode, we find from the electromagnetic part of the Lagrangian Eq.13 by adding dissipative terms and an external oscillator b_d driving the pump mode

$$\ddot{b}_i + \frac{\omega_i}{Q_i} \dot{b}_i + \omega_i^2 b_i = \omega_i^2 V_{cav}^{-1/3} q_l \left(C^l_{ii} b_i + \sqrt{\frac{U_j}{U_i}} C^l_{ij} b_j \right) + J_i + \frac{\omega_i}{Q_i} \sqrt{\frac{U_d}{U_i}} \dot{b}_d \times \begin{cases} 1, i = 0 \\ \epsilon, i = 1 \end{cases} . \tag{14}$$

Here $i = 0$ refers to the pump mode and $i = 1$ to the signal mode, the Q_i are the electromagnetic quality factors of the eigenmodes and U_d the average energy induced by the external drive. The Gertsenshtein current enters as a projected current J_i (see ref. [5] for further details).

From the mechanical part of the Lagrangian in Eq.13 the mechanical EoM is with an additional damping term given by

$$\ddot{q}_l(t) + \frac{\omega_l}{Q_l} \dot{q}_l(t) + \omega_l^2 q_l(t) = \frac{1}{M_{\text{cav}}} (f_l(t) + f_l^{ba}(t)) \tag{15}$$

with the simplified field back-action

$$f_l^{ba}(t) = 2V_{cav}^{-1/3}\sqrt{U_0U_1}C_{01}^l b_0(t)b_1(t), \tag{16}$$

which sources an additional displacement of the cavity shell due to the electromagnetic fields in the cavity. This is also known as Lorentz force detuning. This additional contribution has dissipative characteristic and generally attenuates the mechanical oscillations excited by GW.

4.1 Signal Power

In general, the system of coupled differential equations, Eq.14 and Eq.15, can only be solved numerically. However, if we assume a monochromatic GW propagating in z-direction in the long-wavelength regime, i.e. $\lambda_g \gg L_{\text{cav}}$, and with small mechanical $q_l(t)$ and signal $b_1(t)$ amplitudes, the EoMs can be solved analytically. This yields the total integrated signal power [5]

$$P_{sig} = \frac{\omega_1}{Q_{\text{cpl}}}\omega_g^4 U_0 \left|\frac{1}{2}\frac{\omega_1^2 C_{01}^l(h_+\Gamma_+^l + h_\times\Gamma_\times^l)}{\beta_1\beta_l - \gamma_1\gamma_l} - \frac{\beta_l H(\kappa_1\eta_{01}^E + \lambda_1\eta_{01}^B)}{\beta_1\beta_l - \gamma_1\gamma_l}\right|^2 \tag{17}$$

with the coefficients $\kappa_n := -\frac{\omega_n}{8c^2}(\omega_0+\omega_g)$ and $\lambda_n := \frac{\omega_n^2}{8c^2}$ in front of the dimensionless Gertsenshtein coupling coefficients η_{01}^E, η_{01}^B. The direct coupling coefficients are defined as [5]

$$\begin{aligned}\eta_{01}^E &:= \frac{1}{H\sqrt{U_0U_1}}\int_{V_{\text{cav}}} d^3H_0(\vec{x})\epsilon_0\vec{E}_0(\vec{x})\vec{E}_1(\vec{x}),\\ \eta_{01}^B &:= \frac{1}{H\sqrt{U_0U_1}}\int_{V_{\text{cav}}} d^3H_0(\vec{x})\frac{1}{\mu_0}\vec{B}_0(\vec{x})\vec{B}_1(\vec{x})\end{aligned} \tag{18}$$

with $H_0(\vec{x}) = h_+(x^2-y^2) + 2h_\times xy$. The quality factors Q_{cpl} for the coupling of the readout system and the total quality factor of the system are related via $Q_1^{-1} = Q_{\text{cpl}}^{-1} + Q_{\text{int}}^{-1}$, with the internal quality factor Q_{int} of the cavity defined without the readout system. The resonance terms can be expressed as $\beta_1 := \omega_1^2 - (\omega_0+\omega_g)^2 + i\frac{\omega_1}{Q_1}(\omega_0+\omega_g)$ and $\beta_l := \omega_l^2 - \omega_g^2 + i\omega_g\frac{\omega_l}{Q_l}$, with the mechanical quality factor Q_l. In contrast to recent studies this result includes an additional damping factor $\gamma_1\gamma_l = \frac{1}{M}V_{\text{cav}}^{-2/3}U_0(\omega_1 C_{01}^l)^2$ arising from the back-action of the em fields. The strongest attenuation occurs if the GW frequency is close to the considered mechanical mode with frequency ω_l.

This has the effect that the highest signal power induced by a passing GW is usually not reached if the coupling coefficient C_{01}^l is of order $O(1)$, but rather of order $O(10^{-5})$ in case the GW is on resonance with ω_l. In figure 4 the effect of the damping term $\gamma_1\gamma_l$ on the signal power is shown with respect to the overlap factor C_{01}^l. Additionally, we plot a theoretical strain sensitivity for the ideal MAGO detector prototype which includes noise models derived in ref. [14]. This includes mechanical noise, thermal mechanical noise, thermal electromagnetic, amplifier and oscillator phase noise as independent noise sources. To compute the sensitivity in figure 4 (b) we assume a temperature of 1.8 K and include all simulated mechanical eigenfrequencies shown in figure 3 with similar quality factors $Q_1 \sim 10^6$. For the EM quality factors we use $Q_i \sim 10^{10}$, for the coupling quality factor in a scanning experiment $Q_{\text{cpl,s}} \sim 10^{10}$ and in a broadband experiment $Q_{\text{cpl,b}} \sim 10^5$. We assume further an integration time of $t_{\text{int}} \sim 10^3$ s and an average wall displacement of 0.1 nm.

A general advantage of this experimental approach is the possibility to operate in a scanning or broadband mode: A scanning experimental configuration assumes the detection of a GW on

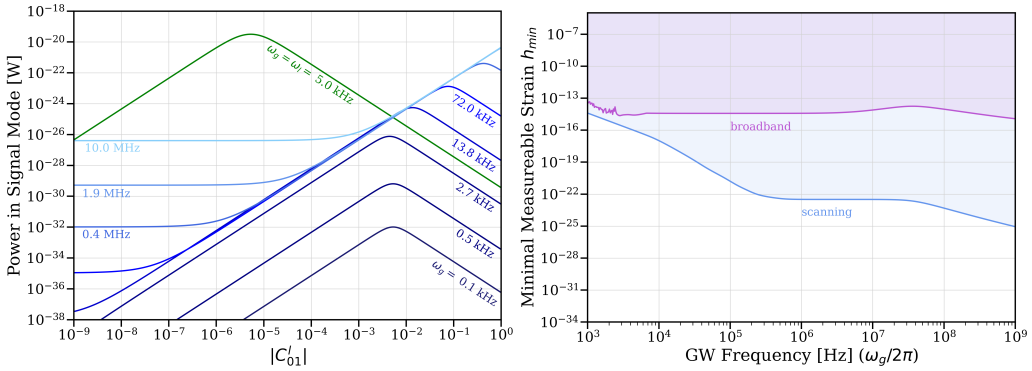

(a) Signal power with damping

(b) Ideal MAGO detector sensitivity

Figure 4: (a) The signal power is not maximized for all GW frequencies with a coupling of order $O(1)$ when the damping term is included in the total signal power, but rather if the coupling is of order $O(10^{-5})$ for GW on resonance. (b) MAGO detector sensitivity calculated for a scanning and a broadband experiment, including the main noise sources: Mechanical, thermal em, thermal mechanical, amplifier and oscillator phase noise.

resonance with the frequency difference of the pump and signal mode, i.e. $\omega_1 = \omega_0 + \omega_g$, where a number of different detectors are needed to span a large frequency range; in a broadband mode the experiment operates at a single fixed frequency difference of the electromagnetic modes and detects GW mainly off resonance such that a single detector could cover a large range of frequencies. A sensitivity comparison is shown in figure 4 (b) and shows that the area of physical interest is in reach for an SRF cavity detector.

5. Outlook

The future of this project is exciting and the goal is to push the strain sensitivity limits further, where theory and experiment go hand-in-hand. Current tests at DESY include measurements of the mechanical and radio frequency modes in a warm environment and first cold tests are planned at the FNAL. Further efforts will aim for the development of a low noise readout system at the desired RF frequency as well as a suitable cryogenic and suspension system. We point out that the general experimental concept reaches still expandable sensitivities in a broadband operation, but quite promising sensitivities in a wide GW frequency range from 10 kHz up to 1 GHz in a scanning experimental setup.

Acknowledgement

We thank the Quantum Universe Cluster of Excellence and the organizers of the EPS 2023 conference.

References

[1] B. P. Abbott et al. “Observation of Gravitational Waves from a Binary Black Hole Merger”, Phys. Rev. Lett. 116 (Feb. 2016), p. 061102

[2] G. Agazie et al. "The NANOGrav 15 yr Data Set: Evidence for a Gravitational-wave Background", Astro. Jour. Lett. 951 (Jun. 2023)

[3] N. Aggarwal et al. “Challenges and opportunities of gravitational-wave searches at MHz to GHz frequencies”. Living reviews in relativity 24.1 (2021), pp. 1–74

[4] A. Berlin et al. "Electromagnetic cavities as mechanical bars for gravitational waves", Phys. Rev. D 108 (Oct. 2023), p.084058

[5] R. Löwenberg et al. "Lorentz Force Detuning in Heterodyne Gravitational Wave Experiments", arXiv:2307.14379 [gr-qc] (2023)

[6] Carlton M. Caves. “Microwave cavity gravitational radiation detectors”, Physics Letters B 80.3 (1979), pp. 323–326

[7] F. Pegoraro et al. “Electromagnetic Detector for Gravitational Waves”, Physics Letters A 68.2 (1978), pp. 165–168

[8] V. B. Braginskii et al. “Electromagnetic detectors of gravitational waves”, Zh. Eksp. Teor. Fiz. 65 (1973), pp. 1729–1737

[9] R Ballantini et al. “Microwave Apparatus for Gravitational Waves Observation”, arXiv: 0502054v1 [gr-gc] (2005)

[10] Ph. Bernard et al. “A Detector of Gravitational Waves Based on Coupled Microwave Cavities”, arXiv: 0203024v1 [gr-gc] (2002)

[11] M. E. Gertsenshtein “Wave resonance of light and gravitational waves”, Soviet Physics Jetp 14 (1962), pp. 84–85

[12] Y. B. Zel’dovich, “Electromagnetic and gravitational waves in a stationary magnetic field”, Zh. Eksp. Teor. Fiz 65 (1973), pp. 1311–1315

[13] A. Berlin et al., “Detecting high-frequency gravitational waves with microwave cavities”, Phys. Rev. D 105, 116011 (2022)

[14] A. Berlin et al., "Axion Dark Matter Detection by Superconducting Resonant Frequency Conversion", arXiv : 1912.11048v1 [hep-ph] (2019)

[15] A. J. Lobo, “What can we learn about gravitational wave physics with an elastic spherical antenna?”, Physical Review D. 52 (1995)

[16] C. W. Misner, K. S. Thorne, J. A. Wheeler, *Gravitation*, Macmillan Education, 1973

[17] G. Goubau, *Electromagnetic Waveguides and Cavities*, Pergamon Press, 1961

[18] M. Maggiore, *Gravitational waves: Volume 1: Theory and experiments*, OUP Oxford, 2007

[19] L.-W. Li, Z.-C. Li, and M.-S. Leong, "Closed-form eigenfrequencies in prolate spheroidal conducting cavity", IEEE Transactions on Microwave Theory and Tech- niques, 51(3):922–927 (2003)